Computers and Electronics in Agriculture 217 (2024) 108599

Contents lists available at ScienceDirect

Computers and Electronics in Agriculture

journal homepage: www.elsevier.com/locate/compag

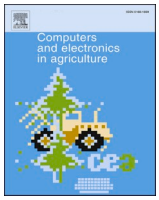

An autonomous Internet of Things spectral sensing system for in-situ optical monitoring of grape ripening: design, characterization, and operation

Hugo M. Oliveira [a,*], Alessio Tugnolo [b], Natacha Fontes [c], Carlos Marques [a], Álvaro Geraldes [a], Sophie Jenne [d], Hans Zappe [d], António Graça [c], Valentina Giovenzana [b], Roberto Beghi [b], Riccardo Guidetti [b], João Piteira [a], Paulo Freitas [a]

[a] INL, International Iberian Nanotechnology Laboratory, Av. Mestre José Veiga s/n, 4715-330 Braga, Portugal
[b] Department of Agricultural and Environmental Sciences (DiSAA), Università degli Studi di Milano, via G. Celoria 2, 20133 Milan, Italy
[c] Sogrape Vinhos, S.A, Rua 5 de Outubro, Avintes, 4527, 4430-809, Portugal
[d] Department of Microsystems Engineering – IMTEK, Gisela and Erwin Sick Chair of Micro-Optics University of Freiburg, Freiburg, Germany

ARTICLE INFO

Keywords:
Grape ripening monitoring
Proximal sensing
Wireless sensor network
Chemometrics
Precision viticulture

ABSTRACT

The present work proposes a novel autonomous Internet of Things (IoT) spectral sensing system for in-situ optical monitoring of grape ripening through reflectance signals. To this end, tailor-made hardware for this IoT end node was developed, characterized, and operated in both lab and field conditions. It included three complementary modules: the optical module, the host module, and the controller module. The optical module included four photodetectors and four LEDs with maximum emission wavelength centered at 530, 630, 690, and 730 nm that was placed in direct contact with the grape berry. The host module included the LED driver and the analog front-end for signal acquisition. Finally, the controller module provided full control of the system and ensured data storage, power management, and connectivity. The system was capable of measuring reflectance in the range of 4 – 100 % with a linear response ($r^2 > 998$) and with a high reproducibility among different optical units. This design made it possible to collect reflectance signals from red (cv. Touriga Nacional) and white (cv. Loureiro) grape varieties in both lab and field environments. The relationship between this optical fingerprint (comprised of the different reflectance intensities recorded) and the evolution of grape berry quality parameters throughout the ripening period (for approximately two months), was analyzed and discussed. Lab data was used to establish a multivariate model based on Partial Least Squares for the prediction of the Total Soluble Solids (TSS) content in both varieties. The model error (Root Mean Square Error in Cross Validation) was 2.31 and 0.73 °Brix for Touriga Nacional and Loureiro, respectively. This model was applied to data acquired in the field in an illustrative example of the potential of the system to predict TSS in real time. The field observations collected during the monitoring period also provided relevant information about the potential issues that may occur during the unattended operation of the optical sensors. Additionally, the modular architecture of the optical module proposed makes it possible to use different LEDs and photodetectors, as well as the assembly of optical filters. This creates the possibility of using the same principles for measuring reflectance in different spectral ranges (e.g. IR) or even fluorescence. The results herein described paved the work for future developments of this technology that will include the development of prediction models for the most relevant grape ripening parameters based on reflectance data, as well as its operation as part of a Wireless Sensor Network.

1. Introduction

The current combination of the challenges posed by climate change and the rapid transformation of the economic value chains is paving the ground for developing a new generation of decision-support systems for viticulture (Pérez-Expósito et al., 2017; Tardaguila et al., 2021). In fact, Precision Viticulture has been growing over the last decades, with advances and applications in multiple areas, from soil quality to selective harvesting (Tardaguila et al., 2021).

One of the most relevant aspects of modern viticulture and

* Corresponding author.
E-mail address: hugo.oliveira@inl.int (H.M. Oliveira).

https://doi.org/10.1016/j.compag.2023.108599
Received 25 August 2023; Received in revised form 13 November 2023; Accepted 26 December 2023
Available online 7 January 2024

winemaking, coined as the synergic "vineyard-winery" alliance, is the quality control of the wine's raw material - the grape (Río Segade et al., 2019), which is the basis for the production of high quality (and valued) wines. The current gold standard of monitoring grape maturation is still based on the manual and random sampling of berries within a block followed by a series of wet-chemistry assays in the lab that imply the destruction of the sample (OIV, 2022). An alternative to the classic lab-based approaches is the use of optical techniques in different agricultural applications (Weiss et al., 2020), from soil and plant status to agri-food products. In the latter case, it is possible to find a strong focus on instrumentation based on NIR technologies coupled with chemometrics techniques (Francisco et al., 2017; Zhang et al., 2021).

New strategies based on optical sensing for monitoring grape ripeness have been also recently reported in the literature. This includes spectral measurements using optical instruments capable of measuring reflectance (dos Santos Costa et al., 2019) or fluorescence (Agati et al., 2007), as well as the proximal imaging of the grapes (Fernández-Novales et al., 2021; Gomes et al., 2021). Other strategies, such as the optimization of the sampling protocol for the wet-chemistry analysis of maturation using satellite Normalized Difference Vegetation Index (NDVI) information (Meyers et al., 2020), have been also reported.

Although all these advances provided a significant evolution from the state of the art, these technologies are still unable to provide real-time information in a fully autonomous fashion. To this end, it is necessary to operate a Wireless Sensor Network (WSN), where multiple end nodes can provide information about the vineyard. This is also a growing topic in precision agriculture, where Internet of Things (IoT) technologies have been changing agricultural production (Xu et al., 2022). The typical IoT architecture deals with the physical devices that generate data (e.g sensors), the network that ensures the transport of the data, followed by the processing of this data to generate meaningful information. The combination of these layers has been exploited in a plethora of agricultural applications that include, crop monitoring, disease prevention, irrigation control, and soil management, among others (Navarro et al., 2020). IoT is also one of the main drives of Precision Viticulture (Ferro and Catania, 2023), where the combination of multiple data sources can create complex tools for monitoring the vineyard (e.g. pest control (Spachos, 2020)).

A potential approach to implement IoT technology in the real-time monitoring of the grape's ripening is the use of simplified spectral sensors as sensing nodes. These sensors include the use of pre-defined spectral bands that can be a source of analytical information about the ripening status of the grape berries. The use of simplified optical devices to measure either reflectance (Giovenzana et al., 2015) or fluorescence (Agati et al., 2013) has been reported in the literature. In contrast to the majority of commercial instruments that measure the light interaction with the sample in a pre-defined continuous spectral range, these simplified instruments rely on the measurement of pre-defined optical bands. This results from the possibility of extracting the most relevant variables from the Vis/NIR reflectance spectra of the grape berries using chemometric tools (Giovenzana et al., 2014). An alternative strategy is based on the multiple interactions of chlorophyll fluorescence with some of the most relevant compounds (e.g. anthocyanins) of the grape ripening process (Agati et al., 2007). Some recent works focused on the downscale of these concepts. This includes the use of prototypes based on commercially available integrated optical components supplied in breakout boards that combine auxiliary electronics, a light source (normally a white LED), and a spectral sensor composed of a photodiode array with integrated optical filters (Pampuri et al., 2021b). This optical configuration allowed the acquisition of multiple reflectance signals that correspond to the spectral bands defined by the bandpass filters (from 450 to 860 nm) using two individual spectral sensors. In this case, the optical bands (number and central wavelengths selected by the optical filters) targeted by these integrated devices were not tailored for these measurements, and some of them have a significant spectral range overlap. Despite their reduced size and the possibility of being part of portable optical devices (Pampuri et al., 2022), the physical configuration of these commercial devices makes them unsuitable to be embedded in the grape bunch, making it impossible to use them as autonomous sensors. Moreover, although these instruments are based on a simplified and downscaled concept, they still require an operator when used either in lab or field environments.

In this context, the objective of this work is to introduce the first version of a prototype of a stand-alone system based on a simplified spectral sensing system that is capable of providing reflectance measurements directly from the grape bunch in a fully autonomous fashion, as originally described in a patent of the authors (Freitas and Piteira, 2018). This system is an IoT device intended to be the end node of a WSN. Taking this context into account, this work has the following objectives: (i) describe the design and development of the IoT spectral sensing system, (ii), characterize the ability of the system to measure reflectance signals, (iii) identify and discuss the main features of the optical signals acquired in both lab and field environments, (iv) develop an illustrative prediction model for Total Soluble Solids (TSS) based on lab data, and (v) show a proof of concept of the application of the prediction model to data acquired in the field by the proposed spectral sensing system. Hence, these objectives pave the ground for the ultimate objective of this work, which is its use for the autonomous in-situ monitoring the chemical parameters of grape ripening, from veraison to harvest.

2. Materials and methods

2.1. Hardware design

To make possible the in-situ optical measurements, the proposed autonomous spectral sensing system acting as an IoT end node (Fig. 1) included three complementary modules: (i) the optical module, which carried the optical sensing elements of the system, (ii) the host module, which carried the LED driver and the analog front-end, and (iii) the controller modules, which ensured the control, power management and IoT connectivity of the whole system. In its current version, each node configuration has a controller and two optical sensor sets, which include two optical modules and their respective host modules (Fig. 1). For lab measurements, a single optical module configuration was adopted.

2.1.1. Optical module

The optical module is composed of four LEDs and four photodetectors assembled onto a substrate. The arrangement of those optical parts is illustrated in Fig. 2. The optical components (LEDs and photodetectors) were supplied by Chips4Light (Sinzing, Germany). LED were purchased in bulk die format, all with similar chip size dimensions of ~ 300 x 300 μm. The LEDs used had a dominant wavelength of 530.3 nm (CREE-C527EZ2290), 637.1 nm (C4L C4L-S12T5), 685.7 nm (Light Avenue LA-AI13WP3), and 730.7 nm (Light Avenue LA-CI13WP3), respectively. Four identical photodetectors (PDs) also in die format, with an area of 700 x 700 μm and a sensitivity in the spectral range comprised between 390 and 800 nm (Light Avenue LA-PD28AP1), were part of the optical layout to collect the reflected light from the sample. The operation point of the PDs was in a short circuit mode (0 V bias). To minimize the stray light of the system, a 3D-printed plastic barrier with 3 mm thickness painted with a mate finishing black ink was placed between the LEDs and the PD array.

Fig. 2 illustrates the optical module prototype that was developed and assembled in two different substrates – flexible printed circuit board (RIGID.flex PCB) and polyimide - that included the same optical components and features. For the flex-PCB, it was used a commercial fabrication process from Würth Elektronik (Waldenburg, Germany), whereas for the polyimide-based modules it was used a substrate fabricated through an in-house process.

For the flex-PCB, the commercial RIGID.flex PCB fabrication process from Würth Elektronik (Waldenburg, Germany) produced a stripe with

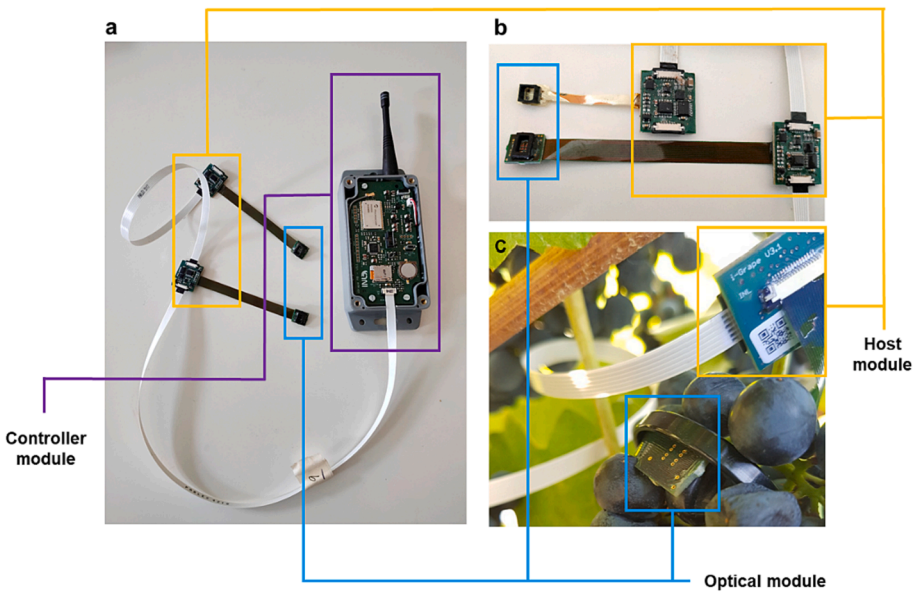

Fig. 1. Internet of Things spectral sensing node with two optical modules (optical sensing heads) (a): detailed representation of two different optical modules (more details in section 2.1.1) connected to a host module (b), and detailed view of the installation of the spectral sensor for field measurements (c).

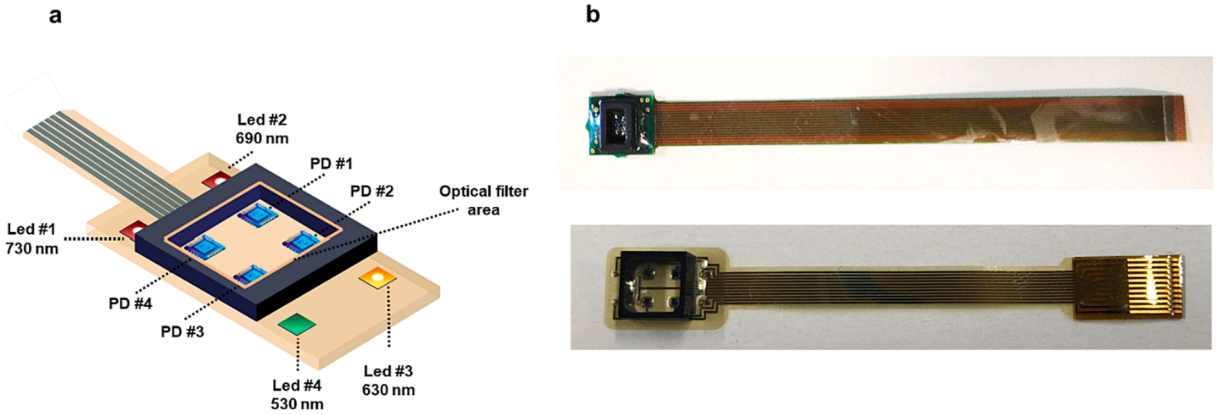

Fig. 2. The optical module of the IoT spectral sensing system proposed. View of the arrangement of the optical components of the spectral sensor (LEDs and photodetectors), as well as the area where a discrete optical filter can be mounted (a), and flex-PCB (top), and polyimide-based (bottom) optical modules (b).

one rigid section (a square two-layer PCB with a side size of 11.5 mm) and a flexible polyimide section with 100 mm length. LEDs were placed outside the barrier while the photodetectors were placed at the center, as illustrated in Fig. 1.

For the flexible polyimide substrate, the in-house fabrication took place on a 4-inch silicon handle wafer to allow parallel fabrication of several sensor units. The process was based on a flexible polyimide substrate obtained by spin coating and the deposition of the conductive tracks. The final assembly is represented in Fig. 2b.

2.1.2. Host module

The host module included the electronics for driving the LEDs and the analog front end to handle the analog signals generated in the optical module. Regarding the LED driver, A LED driver from Semtech (Camarillo, USA) was used to provide a driving capability of up to 50 mA in steps of 31.25 μA. This driver is supplied at 5 V providing enough headroom for the LEDs with higher forward voltage. All LEDs were operated from a 5 V supply, capable of turn-on all LEDs (above forward voltage) with a maximum current of 50 mA.

To handle the analog signals, the host module carries a low-offset, low-drift, and low-noise 4-channel integrated Transimpedance Ampiflier (TIA) (AS89000 from AMS Premstätten, Austria), a channel for each photodetector in the optical module. In this part, each TIA has 8 gain (resistance) settings: 25 kΩ, 100 kΩ, 500 kΩ, 1 MΩ, 2 MΩ, 5 MΩ, 10 MΩ, and 20 MΩ. The TIA output voltage is then fed to an Analog to Digital Converter (ADC) (MAX11614, Maxim Integrated Products, Sunnyvale, USA) with 12-bit resolution. This ADC version (MAX11614) has 8 analog input channels that could be configured for unipolar/bipolar and single-ended or differential mode operation (providing 4 differential multiplexed input channels). The used configuration of the host module was set for unipolar and differential operation (Fig. 3b $V_{out} - V_{ref}$ at the input of ADC) with a supply voltage of 5 V. Converted digital data can be retrieved via the I2C bus ADC interface.

2.1.3. Controller module

The controller module runs software (firmware) capable of controlling the operation of optical and host modules, executing the sequence for optical module data readout, managing system power providing low-power sleep and standby operation modes, and data transmission supported by an IoT connectivity (Fig. 4). The central piece of this system is an ARM Cortex-M0 + microcontroller running at 16 MHz (ATMEL ATSAML21G) with 128 KB flash memory and ultra-low-power

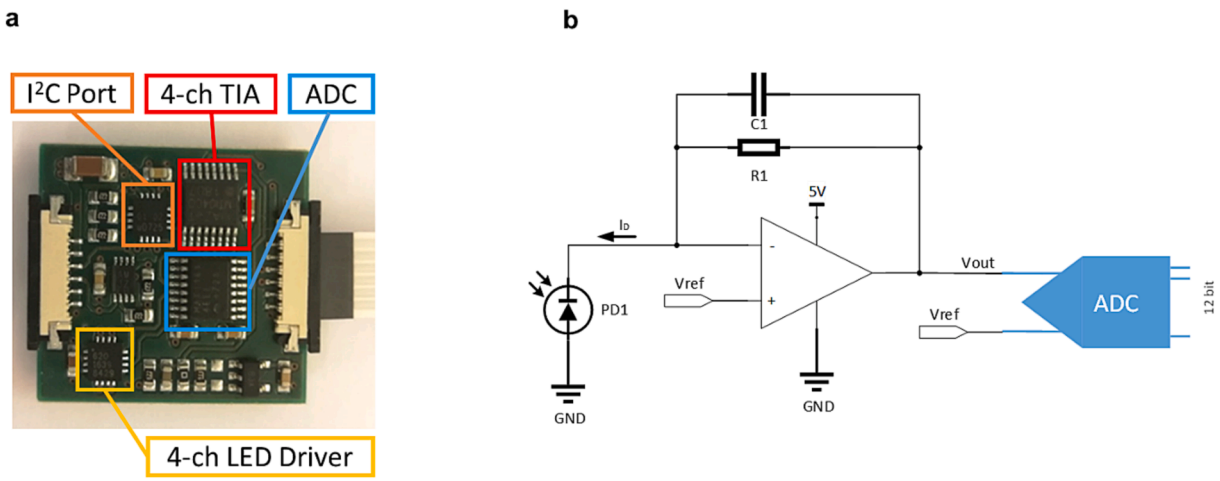

Fig. 3. Host module - LED driver and Photodiode signal acquisition (a), and photodetector signal path - *trans*-impedance amplifier (TIA) with the gain set by R1 and differential input ADC (b).

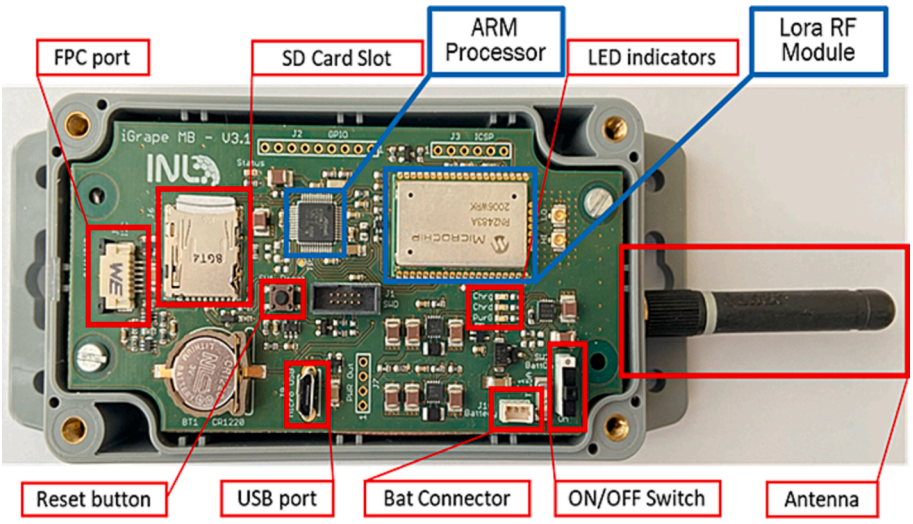

Fig. 4. Detailed representation of the main components of the controller module mounted on an IP67 box.

performance (35 μA / MHz in active mode and 200nA in Sleep mode). Additional features and peripherals such as serial interfaces Serial Port Interface (SPI) and Inter-integrated circuit (I2C), and Real-Time Clock (RTC) are embedded within the microcontroller chip. The controller module was connected to the host module via a serial I2C bus and can support up to four modules with addresses physically set by two bits in the host module PCB.

As for IoT connectivity and data transmission, the Controller module uses the RN-2483A from Microchip which supports Lorawan full stack protocol. This Lorawan module takes on SEMTECH LoRa Transceivers operating in the 868 MHz ISM bands (EU) to provide for low data rate transmission over a 10 to 15 Km line-of-sight range (Xu et al., 2022). The Lorawan bandwidth and modulation configuration was a trade-off between MAC payload size, lower airtime and maximum range. For a maximum allowed payload size (222 bytes) and optimized range, the configuration was set to a spreading factor (SF) 08 and a bandwidth of 125 kHz. The Adaptive Data Rate was disabled and the gain of the used antenna was 1.6 dBi. These settings reduced the bit rate but allowed a larger number of nodes within the network (lower airtime). The central microcontroller firmware prepares data packets from sensor readout data and communicates with the Lorawan module through the serial Universal Asynchronous Receiver Transmitter (UART) port issuing 'Attention' (AT) commands that activate Lorawan functions for joining the network and transmitting data.

For standalone operation, the controller has a Li-Ion battery (Padre Electronics PD655255 with a capacity of 2300 mAh) and a power management hardware section that includes a Li-Ion battery charger (Microchip MCP73833) that charges the battery from the USB port (5 V), two DC-DC converters (TPS63001 and TPS63002) and a RTC battery. The DC-DC converters are two buck-boost regulators that provide the 5 V and 3.3 V supply voltage when operating from the battery. A micro-SD card data storage was included for data persistence/redundancy preventing data losses from RF Lorawan transmission.

2.2. Grape samples

Grapes from cv. Touriga Nacional (TN, red variety) were collected in the winegrowing region of Douro Valley at Quinta do Seixo (Sogrape Vinhos, Tabuaço, Portugal) from late July to mid-September 2020. Within the same period, grapes from cv. Loureiro (LOU, white variety) were collected in the winegrowing region of Vinho Verde, at Quinta de Azevedo (Sogrape Vinhos, Barcelos, Portugal). Each sample corresponded to a random collection of 200 berries from a single vineyard row, from a total of 10 rows of the selected vine-plot, to cover the variability between berries at each sampling time. Then, the analyses were performed in lab scale conditions using the optical sensor to test

(qualitatively and quantitatively) the sensor's optical behavior of each sample in comparison with the reference analysis for the quantification of the Total Soluble Solids (TSS, °Brix) using a digital refractometer.

Therefore, from each of the 200 berry samples, a set of 30 berries was analyzed optically and the entire amount of 200 berries (with the 30 included) was then analyzed for the TSS quantification after mixing (30 s using a home blender) and filtering of each sample bulk.

The samples were collected on 6 different days for TN and 4 different days for LOU (for a total of 76 and 42 samples, respectively). The complete calendar of the sampling campaign is available in Table S1 as part of the Electronic Supplementary Information (ESI).

In addition, one node was placed directly in the field (Quinta do Seixo, Sogrape Vinhos, Tabuaço, Portugal) to autonomously monitor the ripening evolution of cv. Touriga Nacional daily (Fig. 5). Each optical module pointed an individual grape directly at the grape bunch. The node measured from the 23rd of July to the 16th of September (from the onset of ripening – veraison, to harvest).

2.3. Optical data collection and processing

Two complementary modes to measure the reflectance signals from the grapes in both lab and field environments were adopted. In the first case, after field sampling, the analysis in the lab environment was performed by placing each berry on top of the optical sensor (onto the optical barrier) and covered by a black plastic case (Fig. 5). In the case of field measurements, the sensors were placed into the grape bunch, in direct contact with a single grape berry. A plastic cable tie was used to minimize the potential movements of the optical modules due to external factors. Eleven measurement cycles were recorded each 30 min, from 00:00 to 05:00, comprising a total of 11 measurements per day. The measurements were taken during the night period to minimize potential background issues caused by ambient light and dark current (related to the high temperatures). Reference reflectance spectral data was collected from individual grape berries using a Jaz Modular Optical Sensing Suite (OceanOptics, Dunedin, FL, USA).

The sensor and grape conditions in terms of grape berry integrity and sensor position were evaluated concurrently on the field sample collection dates along the monitoring period (t0, t1, t2, t3, t4, and t5) according to five qualitative attributes: (i) berry in very good conditions, (ii) berry in good conditions, (iii) berry in fairly good conditions, (iv) berry in compromised conditions, and (v) berry in extremely compromised conditions. Such attributes were used as a qualitative label to evaluate the meaning of the data in the unsupervised explorative data analysis (description below).

The optical measurement cycle consisted of the illumination of the berry with each individual LED followed by the signal acquisition for each photodetector, turning on and off each LED in a sequencing cycle with the corresponding readout by the four photodetectors. At the end of the four LEDs turn ON cycle, a final acquisition without any illumination was performed to screen the influence of potential background light. Therefore, each measurement cycle consisted of 20 readouts (each individual readout corresponded to an average of 16 acquisitions). The Signal to Noise ratio (SNR) of the photodetector's signal chain is optimized for each measurement by an Automatic Gain Control (AGC) algorithm which sets the amplifier (TIA) gain for maximum SNR. The resulting readout can be normalized by dividing by the gain setting for each measurement. For the field measurements, the nodes were set to perform the analysis overnight following the same measurement cycle and repeated 11 times per day (every 30 min, from 00:00 to 05:00). The same procedure was also used to calculate the normalized sensor readout.

In post-processing, given the need of an analytical approach capable to extract chemical information from 20 optical data of each measurement cycle, the sensor readouts were analyzed following a chemometric approach. For this reason, the two data matrices (composed by 76 and 42 samples of TN and LOU, respectively) were arithmetically autoscaled column-wise (substracting the column mean and dividing by the column standard deviation eanch value of each column, equation (1) to give the same importance to all the optical outputs.

$$\widehat{x_i} = \frac{x_i - \overline{x}}{std(x)} \tag{1}$$

where $\widehat{x_i}$ is the autoscaled value, x_i is the original value of a data point, $\overline{x_i}$ is the column mean of the optical variable and $std(x)$ is the column standard deviation of the optical variable.

Then, the Principal Component Analysis (PCA, usupervised method based, in this case, on singular value decomposition) was applied to explore variability retained in both lab and field optical data to detect any possible source of information related to the grape ripening profile.

Afterward, using the lab data, a linear modelling based on the Partial Least Squares regression (PLS) method (which maximizes the covariance among the optical readouts and the wet-chem reference analyses (TSS)), was carried out to calibrate a predictive model for TSS quantification (Tugnolo et al., 2021; Wold et al., 2001). Model accuracy was evaluated (in calibration and cross-validation) using the RMSE (Root Mean Square Error), as well as bias and R^2 (coefficient of determination); the lower

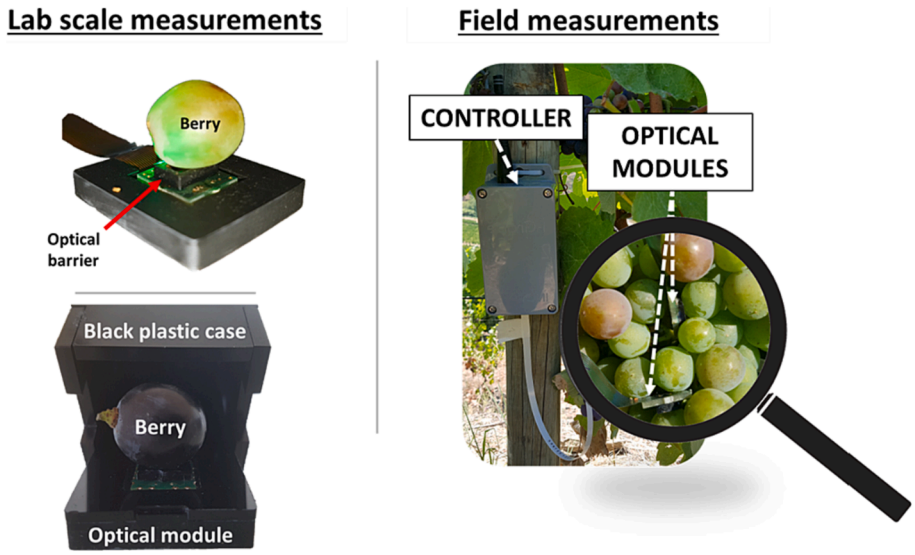

Fig. 5. Configuration of the optical module for performing optical measurements in both lab and field environments.

the error and the bias and the higher the R^2 (as maximum equal to 1), the better the model performances. Once calibrated, the model was applied for field measurements to have a first screening of the sensor applicability in field.

The entire data process was performed in Matlab® environment, version 2020b (The MathWorks, Inc., Natick, MA, USA) using both the PLS-Toolbox package (Eigenvector Research, Inc. Manson, Washington) and in-house functions (both Matlab built-in functions and self-made operations for sensor raw data management).

3. Results and discussion

The IoT spectral sensing system proposed here considered three major aspects: (i) installation and operation compatible with the deployment of the sensor inside the grape bunch, (ii) operation in both lab and field environments, and (iii) full autonomous operation for the complete ripening season after deployment. Thus, it was necessary to design a flexible optical substrate with a dimension of ~ 12 x 12 mm where the optical components were installed. The system was also envisioned to operate not only in the field environment but also in the lab due to the need of develop the calibration models. This implied the control of a different number of sensors for each particular case (two optical modules per controller for field operation and one module in the case of the lab operation). In the case of the lab operation, the data transmission was switched off. Finally, a strong effort in the power management of the system was needed to minimize the power consumption per measurement cycle. This strategy ensured the operation of the system for the complete ripening season without recharching or replacing the battery. Additionnaly, the system was designed considereding its potential scability at an afforable cost, which is a key feature for future upscale and deployment of the proposed end-node in a WSN.

3.1. Design of the optical module

The use of the optical properties of the grapes to predict their ripening quality parameters has been performed by benchtop and/or portable instrumentation (mainly by manual operation) to acquire the diffuse reflectance signals as a full spectrum in the Vis/NIR range (Ferrara et al., 2022; González-Caballero et al., 2012). To simplify this scenario, which makes it impossible to upscale these applications due to the high cost of the instrumentation and its respective operation, previous research also reported simplified instrumentation based on selected optical bands (Giovenzana et al., 2015) (Pampuri et al., 2021b; Ribera-Fonseca et al., 2016).

This simplification was based on the most relevant spectral changes that are associated with the quality parameters of the grapes during their ripening stage. During the crop season, relevant variations in the green region (around 530 nm) are noticeable from veraison to harvest due to the grape berry pigmentation (development of anthocyanins, in red grape varieties, and disappearance of greenery) (Agati et al., 2008). The same variation is noticed also around 680 nm, associated with the chlorophyll absorption peak, which also degrades with the development of sugars and anthocyanins (Rocchi et al., 2016). In the short wave near-infrared region, a maximum reflectance peak is shown around 730–750 nm related to the third overtone of –OH bond stretching. Changes related to the development of sugars and the decrease in water content are well correlated to the absorption of this overtone (Giovenzana et al., 2014). Based on this background, our band selection included four optical bands in the Vis/NIR range highlighted in Fig. 6. These bands corresponded to the dominant wavelength of the LEDs used to build our prototype: 530, 630, 690, and 730 nm. Due to the importance of chlorophyll degradation in the grape ripening process, a second optical band (centered at 630 nm) around the absorption peak of the chlorophyll was added.

To collect the reflected light from the sample, PDs with a sensitivity compatible with the target reflection signals, from 500 to 800 nm, and a sensitive area of 0.27 mm^2 as part of the optical module were used. An array of four PDs was managed to add redundancy to the measurement setup. A 3D printed optical barrier (with external dimensions of 9.0 x 6.0 x 3.0 mm) was placed between the LEDs and PD array to minimize the stray light that reached the photodetector (footprint illustrated by a red line in Fig. 1). These optical components and the barrier were assembled in two different substrates: flex-PCB and polyimide. Although measurements were possible using both sensors (that also assured the flexibility needed for installing the sensor into the grape bunch), the following results were based on the flex-PCB-based sensors. This is due to its easier scalability, which was a key aspect of producing several units for both lab and field testing. The proposed layout is also comprised of a modular architecture that can accommodate different LEDs and photodetectors. Hence, it can be used not only to measure the direct light interaction with the grapes (Jenne and Zappe, 2023) for reflectance measurements but can also be adapted to other applications with minor modifications. For example, photodetectors (Fig. 2a) can be fabricated on different materials that modify the sensitivity of the detection in the Vis range (e.g. a-Si:H and CMOS) or cover the IR (e.g. InGaAs). The same rationale applies to the LEDs used for illumination (Fig. 2). Additionally, it is also possible to include optical filters on top of PDs in either discrete or integrated configurations. In the former case, the filter can be installed inside the cavity provided by the optical barrier, whereas in the latter case, the filter(s) can be monolithically integrated into the PD (Nikolaidou et al., 2022b). This feature makes it possible to perform fluorescence measurements based on the same architecture of the optical module.

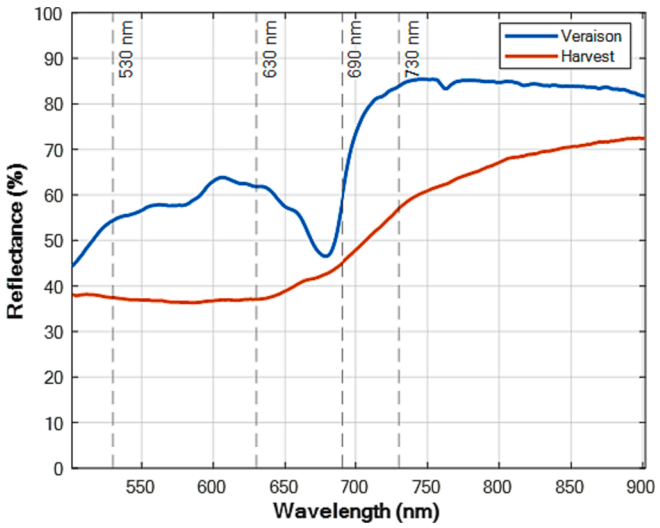

Fig. 6. Vis/NIR reflectance spectra of a grape (cv. Touriga Nacional) collected at veraison (t0) and harvest (t5) collected by a commercial spectrometer (Jaz Modular Optical Sensing Suite, OceanOptics, Inc., Dunedin, FL, USA).

3.2. Design of the host module

The host module had two fundamental functions: to drive the LEDs used as light sources to illuminate the grapes, and to condition the analog signals generated by photodetectors (Fig. 3a).

The hardware design of the LED driver section in the host module has to meet the LEDs maximum drive current and their corresponding forward voltage. The four LEDs (presented in 2.1.2) due to their physical nature (various monochromatic wavelengths) have intrinsically four different forward voltages. The forward voltage of a LED is the voltage drop at its terminals that allows current to pass through the LED to emit light. The detailed characteristics of the different LEDs are available in Table S2.

To get a constant light-intensity from a LED, it should be driven with

constant-current, which is the role of the Semtech LED driver. Since the maximum current driving capability of this driver is 50 mA, we have set the forward current at 50 mA in all LEDs for maximum luminous intensity, which means that in some cases the forward voltage will be slightly higher than the nominal value defined for each LED. The highest forward voltage has been set by the 530 nm LED that with a 50 mA forward current corresponds to 3.6 V, thus requiring a 5 V power supply in the host module to have enough headroom for LED operation. All remaining LEDs will operate well below that value, in the range of ~ 2 V forward voltage.

Four identical photodetectors (PDs) were assembled with the four LEDs (Fig. 2). The reflectance measurements have to detect low-luminance optical signals that generate low-level photocurrents in the range of pA to μA at the output of the photodetector. In precision optical sensing, a direct conversion between the photocurrent and the output voltage is usually made with a *trans*-impedance amplifier (TIA), having the photodetector in photovoltaic mode with zero-volt biasing (or with a negative voltage bias).

Without any illumination, these photodetectors generate a very small current, in the range of pA (also known as dark current), but as light intensity increases this current can be in the order of μA. A classical resistive Trans-Impedance Amplifier (TIA) topology was used in this design with V_{ref} setting the photodetector biasing voltage as shown in Fig. 3b (V_{ref} can be a zero or negative voltage). A programmable feedback resistor sets the gain in this TIA topology (AS89000 with 8 gain settings), generating a voltage output to be digitized by an Analog to Digital Converter (ADC), thus maximizing Signal-to-Noise Ratio (SNR), despite the feedback resistance thermal noise. The selection of ADC was made on the assumption of a very low sampling rate operation to reduce power consumption and also optimize the overall SNR in the readout signal chain. Operating at a 5 V power supply, the ADC power consumption is extremely low at a low sampling rate: 670 μA@94.4 ksps.

3.3. Design of the controller module

The main function of the controller module is to generate the readout sequence of the optical sensor from each set of host module/optical modules, to process the acquired data, store, and wirelessly transmit this data into an IoT database (the detailed operation sequence is described in the ESI section "Operation sequence and power consumption of the controller module"). In addition to this function, the hardware has been optimized to meet low power consumption and data persistence, as well as provide long wireless range transmission. The central piece of this hardware is the ARM processor ATSAML21G (ARM Cortex-M0 +), which runs at 16 MHz and has 128 KB flash memory being enough to accommodate all the firmware code and acquired data. It has low power features as low as 35 μA/MHz in active mode and 200 nA in sleep mode. This contributed to low power consumption when the complete system is in sleep mode, which is the dominant operation mode throughout the measurement cycle. Connected to this microcontroller, there is a set of peripherals interfacing through serial synchronous interfaces (SPI and I2C) and a UART serial port (for the AT commands) that complete the necessary functionality for this controller (Fig. 4), such as a LoraWAN module, a SD card reader slot, a RTC battery, and a system battery. The operation sequence and its respective power consumption are detailed in Table S3. The estimated daily average power consumption for the daily data acquisition cycle was estimated to be less than 15 mA per operation day, which translates to a requirement of at least 1800mAh system battery in a 4 month season duration (~120 days, June to September). The battery was sized with a capacity of 2300 mAh which is enough to cover those power consumption requirements without recharging the battery during the season (from deployment/installation to harvest time).

3.4. Hardware operation and digitalization flow

The workflow of the proposed system is illustrated in Fig. 7. The first step to operating the system in a fully autonomous fashion consists in its field deployment. Hence, the field installation consisted in inserting each individual optical module into the grape bunch, pointing directly to one grape. To minimize potential movements of the optical module, plastic cable ties were used to hold the flat cables (e.g. picture of the graphical abstract). After the physical attachment of the optical modules to the grapes, a priming measurement cycle was run to test the measurement cycle and the data transmission. After this step, the installation was concluded and the system slept until the first alarm was triggered to start the measurement cycle (up to 18 alarms could be preset).

After running a measurement sequence, the raw data was stored in the SD card and a compressed payload of this data is transmitted to a IoT network server (MQTT – Message Queuing Telemetry Transport broker). Then, this payload is uploaded in a database, followed by its analysis by the pre-trained models contained in the software app.

Due to the complexity of the several layers involved in the complete application, the present work focused on the hardware side and its capabilities to be an autonomous end node for grapes' ripening monitoring. Therefore, all detailed aspects related to the development and the use of the prediction models, in addition to the operation of the nodes in a WSN are out of the scope of the current work and will be presented elsewhere.

3.5. Grape berries ripening reference analysis and optical measurements in lab environment

Table 1 summarizes the descriptive statistics related to the grape wet-chem reference analyses (TSS) carried out on the two varieties taken into consideration (TN and LOU). Overall, a significant variability has been observed for both grape varieties, and TN showed quite high TSS values at the end of the sampling campaign since is one of the red grape varieties used for the production of fortified wines (i.e., Port wine).

Beyond the hardware perspective detailed in section 3.1, the optical prototype was designed to accommodate a good compromise among the existing optical indexes for grape ripening monitoring, the application in a real scenario, and the technical requirements of an IoT stand-alone sensor (e.g. power management and data payload). These sensors were characterized in a lab environment using reflectance standards (a detailed explanation of the characterization and its respective results is available in the ESI section "Characterization of the reflectance measurements", Table S4 and Fig. S1-S4), being able to perform consistent reflectance measurements from 4 to 100 % in the optical bands of interest. Fig. 8 shows the optical readouts of the two grape varieties (TN and LOU) collected in the lab during the season 2020. The optical outputs were rearranged to show the grape berry optical signature acquired from each photodetector (labeled as channel – ch – for the sake of simplicity) at each LED, including the signal with all LEDs switched off (background signal). At a glance, a different evolution of behavior is noticeable from Fig. 8a to Fig. 8b, strictly related to the nature of the red grape variety (TN), which acquired a purplish color right after the second sampling session (t1 (Aug-05), Fig. 8a). Conversely, the white variety LOU maintains a higher reflective capacity showing a yellowish coloration till the moment of harvest (t3 (Sep-17, Fig. 8b).

These differences are related to the concentration of anthocyanins, in the case of red grape varieties. Indeed, these phenolic components are absent in LOU while they increase over time (from *veraison*, t0, to harvest, t5) for TN leading to low reflectance values, especially at 530, 630, and 690 nm.

Since the final goal of the stand-alone prototype is to predict different maturation parameters using reflectance signals of four discrete optical bands, the "maturation indexes" (developed using the ratio between reflection signals at different optical bands (wavelengths)) reported in the literature (e.g. (Giovenzana et al., 2014; Ribera-Fonseca et al.,

Fig. 7. Digital workflow of the proposed spectral sensing system.

Table 1
Descriptive statistics of the Total Soluble Solids (TSS) analysis obtained from cv. Touriga Nacional (TN) and cv. Loureiro (LOU) samples through the laboratory reference method.

TSS (°Brix)							
variety	number of samples	mean	std	min	max	skewness	kurtosis
TN	76	3 [a]	7.05	7.00	33.70	−0.49	2.21
LOU	42	1.55[b]	1.84	13.34	20.30	−0.70	2.52

std: standard deviation

2016)) have limited predictive performance for the sensors placed inside the grape bunch. This is due to the intrinsic characteristics of the field conditions that include scattering effects, uncontrollable optical path, tissue heterogeneities, instrumental noise, and environmental effects (e.g., rain, wind, plant infections), among other sources of variability.

This was bypassed by adopting a multivariate-based strategy capable of extracting useful chemical information related to the ripening profile leaving the noise sources outside the data computation. Therefore, PCA was applied to explore the data acquired in lab-scale conditions that was affected by collinearity. The readouts related to the signals registered from each channel with the LEDs off (background) were excluded from the dataset used for PCA because they were not considered significant and influential during the calculation (recorded values with a value of ~ 0 counts).

Fig. 9 shows the PCA outcome (scores and loadings) for TN. In this case, to better display the results, PCA scores were represented against the sample number associated with the TN dataset (sorted by sampling time). PC1 (Fig. 9a) describes 88 % of the total information included in the TN dataset. Two main clusters can be highlighted from positive to negative values of PC1, which represent the color change of the berries associated with the ripening process (from green to purple) that occurred from t0 to t1-t2. This behavior was confirmed by the constant positive loadings of PC1 (Fig. 9c) related to the constant decreasing reflectance trend of the grape samples (due to the anthocyanin accumulation) during the ripening process. Additionally, PC2 (Fig. 9b) describes approximately 8 % of the total variability. PC2 shows an interesting increasing trend (from negative to positive values) related to the ripening process which occurs after veraison (t1-t2). The loadings of

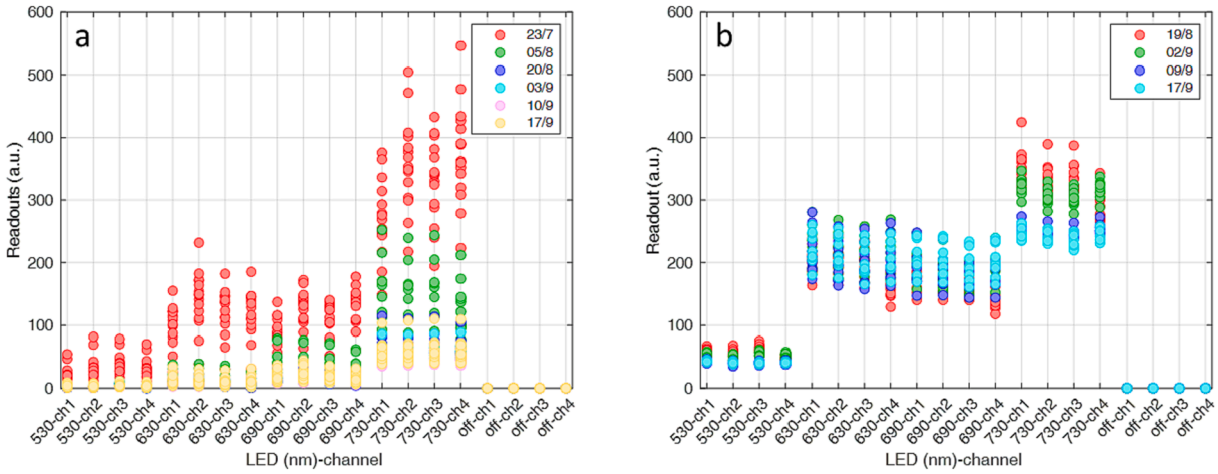

Fig. 8. Reflectance readouts (raw data) of each LED (530 nm, 630 nm, 690 nm, and 730 nm) photodetector (ch1, ch2, ch3, and ch4) combination, as well as the background signal (labeled as off). Readouts were obtained from grape berries samples of (a) cv. Touriga Nacional and (b) cv. Loureiro (b) at different times (marked as samples' labels) of the ripening period.

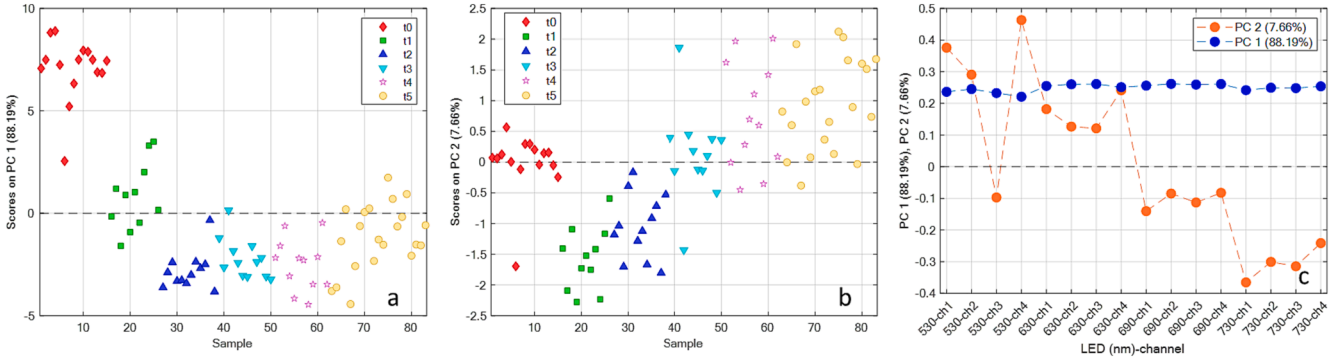

Fig. 9. PCA scores and loadings of the optical data acquired in lab scale for TN: PC1 scores plot (a), PC2 scores plot (b); PC1 and PC2 loadings plot (c).

PC2 show (Fig. 9c) an indirect relation between 530——630 nm, and 690——730 nm, which is ascribable to the increasing concentration of anthocyanins components and the degradation of the chlorophylls (Song et al., 2021).

Fig. 10 shows the PCA outcomes of the optical data from LOU samples acquired in lab-scale conditions. Differently from the red variety, the ripening process can be described by the variability collected only by the first PC (variance explained equals 51.22 %). Indeed, a clear evolution trend comes up from positive to negative values of PC1 (Fig. 10a) indicating the four sampling sessions from *veraison* to harvest. The variables contribution (loadings) for the description of PC1 (Fig. 10b) indicates an opposite relation of the LEDs at 530 nm and 730 nm with the LEDs at 630 nm and 690 nm. This behavior is strictly related to the degradation of the chlorophylls (properly described by the variables at 630 and 690 nm) and the water content along the time (detected by the channels at 730 nm ascribable to the third overtones of O–H stretching in water) (Ercoli et al., 1993; Pampuri et al., 2021b).

Fig. 11 shows the figure of merit measured against predicted samples using PLS models for the TSS parameter, for both TN (Fig. 11a) and LOU (Fig. 11b). Regarding R^2 and RMSE, it is interesting to underline the minimal differences between the performance of the models in calibration and cross-validation (CV) suggesting a good robustness of the models using internal validation. Concerning the model goodness, a good performance in terms of model error (RMSECV) was obtained for the TSS estimation. Indeed, an average of 2.31°Brix and 0.73°Brix were obtained as model errors for TN and LOU, respectively. Such performance, if maintained also in field scale, could be improved due to the deployment of several nodes, which can simultaneously provide an average estimation of the vineyard condition with a reduced experimental error.

3.6. Grape berries optical measurements in a field environment

All technical developments have been made considering the application of the sensor under real conditions. Therefore, Fig. 12 shows the field optical data collected from TN by one optical module placed in the field, in a commercial vineyard.

The field optical data (recorded with LEDs off) were affected by environmental light pollution (background different from 0). Therefore, the raw optical data matrix has been mathematically pre-processed to reduce at best the background effects. In detail, from each readout with LED switched on (the reflectance reading of each LED at each channel) the corresponding background value was subtracted. The 11 acquisitions performed every single night were averaged to obtain a single optical output which is representative of a single day of measurements of a pre-defined grape bunch. Then, the new data matrix was explored with PCA and used as input data for the PLS model developed in the lab.

Fig. 13 shows the PCA outcomes performed on the pre-treated field data. Also, in this case, PCA scores were (Fig. 13a and b) represented by the sample number associated with the TN dataset which is representative of the day of monitoring. During the field sample collection dates along the monitoring period (grape berry ripening period), the physical conditions of the monitored berries were visually evaluated (as grape qualitative label) at different times (t0, t1, t2, t3, t4, and t5). Such empiric assessment of the berry status by visual inspection (without any relationship with the chemical parameters) was used to detect significant modifications in the optical signals. This approach was followed during each sampling day in the lab and allowed to verify the reliability of the field data collected during the field experimental season. Indeed, if the conditions of the berries were non-compliant (e.g., dehydrated, damaged, etc.) or the optical module was not in the correct position (optical module too far from the target or out from the bunch), the latter was being rearranged into the same grape bunch in the correct location.

The PC1 and PC2 scores and loadings followed the same behavior as the TN data collected in lab conditions. Indeed, PC1 (Fig. 13a) shows the grape optical trend from greenish to purplish, while PC2 (Fig. 13b) shows an increasing behavior from August 1st until the harvest, which is consistent with the data collected in the lab. However, at t2, t3, and t4, the sensor was rearranged in the grape bunch due to the conditions of the berries that have started to dehydrate causing an incorrect positioning of the optical module into the bunch. We also observed a significantly different score on the 21st of August when compared with the neighboring days. Such an event was related to rainfall which caused an accumulation of moisture around the berry obtaining reflection effects that were abnormal and unrelated to the actual internal chemical characteristics of the berry.

Finally, to have a first screening of the sensor applicability in field, the PLS model calibrated in the lab was applied for field measurements. Fig. 14 shows the daily TSS prediction for the whole monitored ripening period (from late July to mid-September). Overall, although some technical and modelling aspects still need to be studied and refined for a real field application, the trend follows the common ripening curve for TSS accumulation. The evolution process appeared coherent till the 18th of August then some events, described (qualitatively) during the analysis of the principal components, influenced the prediction of the results. Indeed, on the 21st of August, the rain caused a clear TSS overestimation. Then, the trend restarted to grow steadily but with TSS predictions slightly below the estimation reached on the 17th of August. Moreover, two trend modifications appeared during the day after the field sampling suggesting a possible change in the estimation caused by

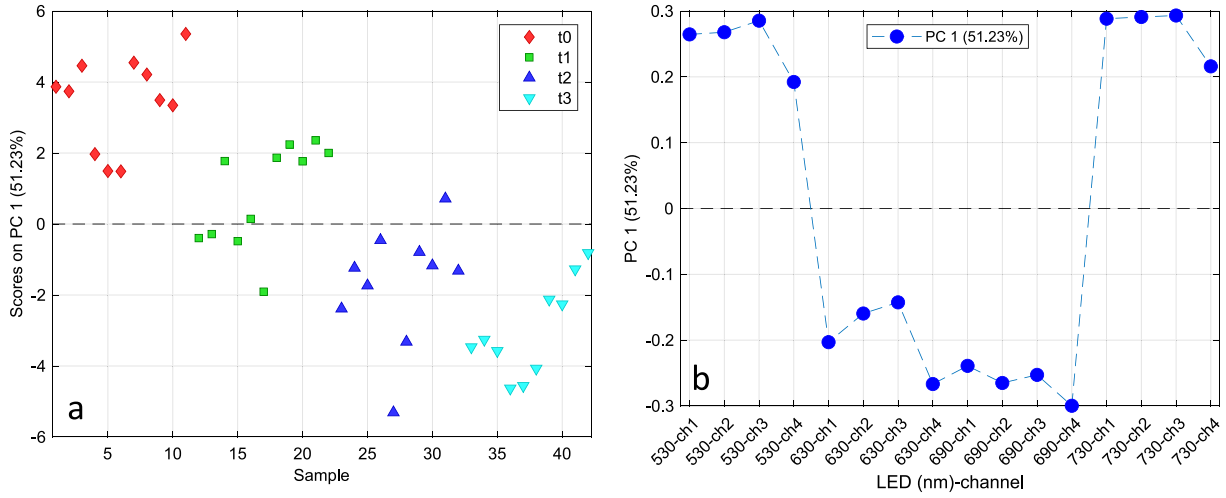

Fig. 10. PCA scores and loadings of optical data acquired in lab scale for LOU: (a) PC1 scores plot, and (b) PC1 loadings plot.

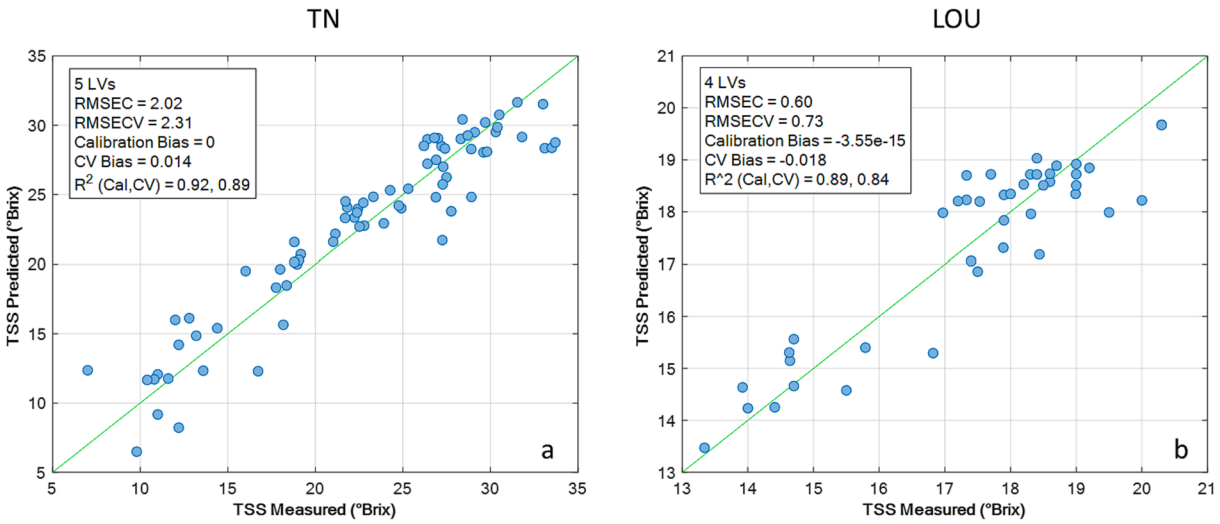

Fig. 11. Values of Total Soluble Solids predicted by the PLS model based on optical lab data vs. values measured through the reference method for the varieties (a) Touriga Nacional (TN) and (b) Loureiro (LOU).

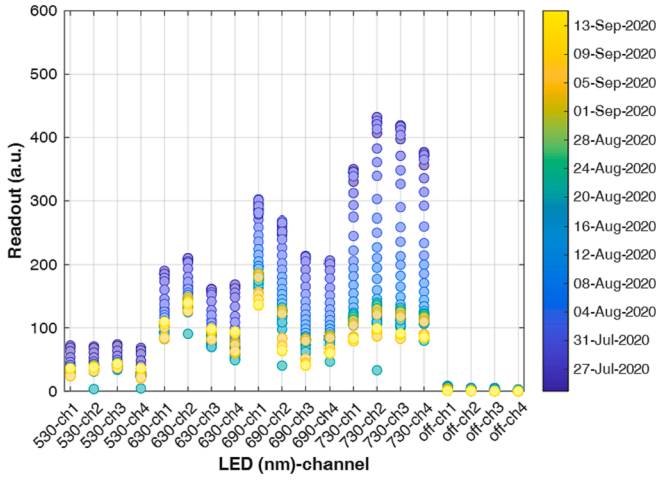

Fig. 12. Reflectance readouts (raw data) of each LED (530 nm, 630 nm, 690 nm, and 730 nm) - photodetector (ch1, ch2, ch3, and ch4) combination, as well as the background signal (labeled as off) obtained from one optical module deployed in the field for monitoring Touriga Nacional grapes during the ripening period.

the operator's intervention to check the sensor conditions.

3.7. Comparison with the current state of the art

The current state of the art for monitoring grape berry ripeness has been driven by the need to develop robust systems capable of monitoring the grape ripening process, and ultimately supplying information able to support the harvest decision. Although the literature reports some examples based on technologies that require sample destruction (Garcia-Hernandez et al., 2018), the recent methodological advances include analytical strategies based on the use of different optical technologies that correlate the optical properties of the grapes with the chemical parameters of oenological interest (Ferrara et al., 2022; Vrochidou et al., 2021). These advances have been essentially supported by spectroscopic and imaging instrumentation developments, with a particular emphasis on miniaturization.

Portable spectrophotometers are widespread on the market, becoming attractive tools for capturing optical data from grapes (Ferrara et al., 2022). These instruments provided detailed optical information in Vis/NIR ranges (namely full reflectance spectra) that can be then used to build predictive models using chemometrics. More recently, simplified instruments based on the measurement of optical bands have also been proposed. One example is the use of a miniaturized commercial spectral sensor to acquire pre-defined reflectance bands from grapes (Pampuri et al., 2022). Another example is the commercial analyzer Multiplex, which is based on multiple fluorescence bands that are part of a series of indexes that allow the quantification of different parameters of the ripening process (Agati et al., 2007). A significant drawback of this fluorescence instrument is its high cost. For example, in a recent economic assessment made for the Multiplex instrument (Savi et al., 2019), the economic viability for a two-hectare vineyard cultivating three red grape varieties (90 samples per year) implied a lifetime of the instrument of at least 7 years, without any additional sampling points. Additionally, these analytical strategies on portable instrumentation also require human intervention in the field to acquire optical data, contributing to increased labor costs, and is especially troublesome considering the lack of manpower that the agricultural sector is already facing.

Another emerging research line is the use of Machine Vision techniques (Vrochidou et al., 2021), which include the use of color, hyperspectral, and NIR imaging. One example was recently proposed by Fernández-Novales et al. (Fernández-Novales et al., 2021), which included the use of a Vis/NIR hyperspectral camera mounted in the front part of an all-terrain vehicle. The images acquired at 5 km/h provided more than one million spectra per sample. After identification of the region of interest (the part of the image corresponding to the cluster), the averaged reflectance spectrum was used to build the prediction models for several parameters (Titrable acidity, pH, Tartaric acid, Anthocyanins, and Total Polyphenols).

In contrast to the above-mentioned analytical strategies, the integrated system proposed here is a stand-alone optical sensing unit that can act as an individual node in a WSN. This makes it possible to have a fully autonomous system capable to monitor the grape in real-time with an almost absent human intervention (an operator is only required for installation and uninstallation of the sensors in the field) in a non-destructive fashion. The development strategy adopted here addresses the upscaling of the solution using micro and nanofabrication technologies that make possible the production of the optical instrumentation at a reduced cost in volume production. Nevertheless, some potential challenges in the field operation of the system can be anticipated. The first is related to the positioning of the sensor, which may vary during the season due to modifications in the grape berry (e.g. dehydration,

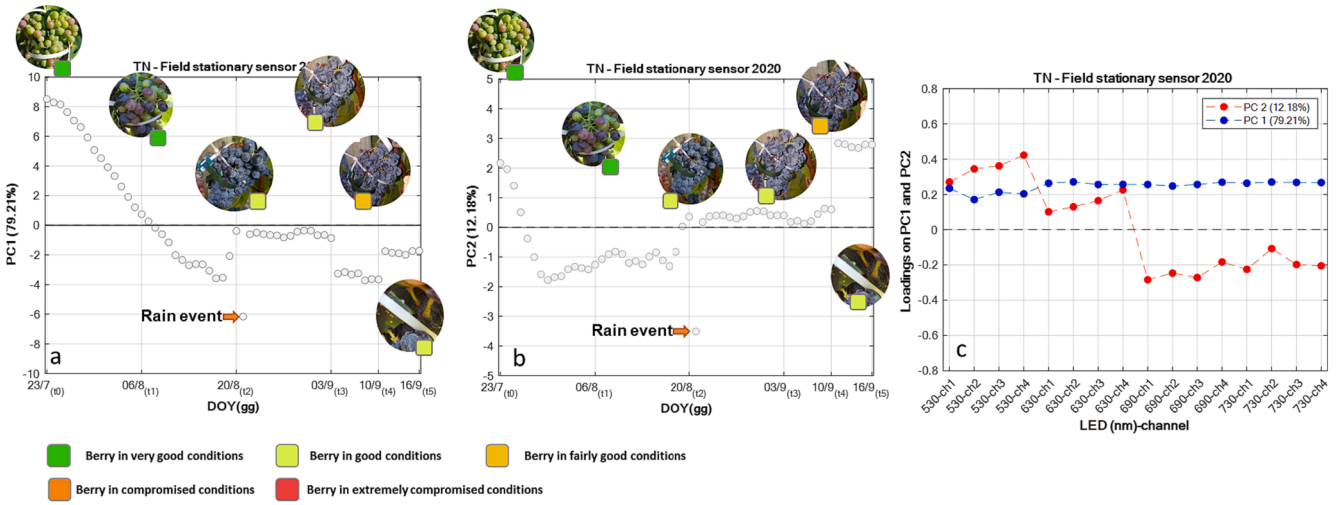

Fig. 13. PCA scores and loadings of field data acquired from an optical module (Touriga Nacional (TN)): (a) TN PC1 scores plot, (b) TN PC2 scores plot, (c) TN PC1 and PC2 loadings plot. Qualitative labelling: (i) berry in very good conditions, (ii) berry in good conditions, (iii) berry in fairly good conditions, (iv) berry in compromised conditions and (v) berry in extremely compromised conditions.

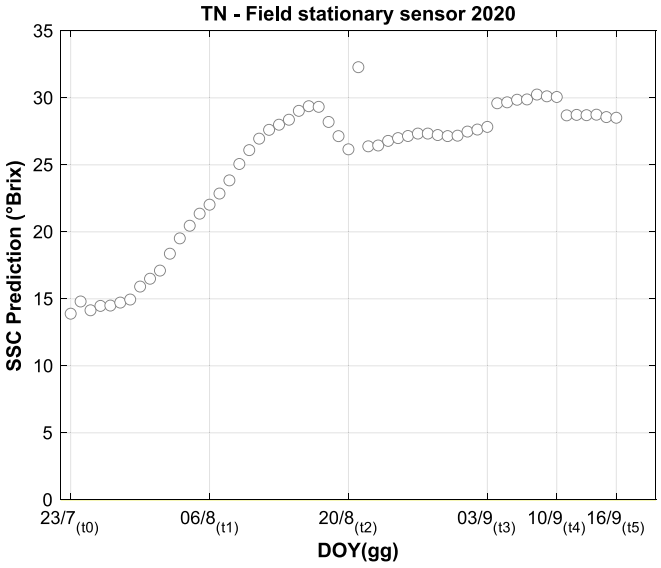

Fig. 14. TSS prediction from an individual optical module for the Touriga Nacional (TN) variety during the crop season.

weather conditions). A second challenge is related to the number of sensors required to monitor a pre-defined area, which is still an open question. Finally, the use of the prediction models built in one crop season in the predictions of the following year may also be challenging in the case of significant differences in the grape's ripening evolution among the different years.

4. Conclusions

The present work describes a novel IoT spectral sensing system capable of autonomously collecting reflectance signals directly from the grape berry. It includes three major blocks: an optical module that interacted directly with the grape berry, a host module that drove the LEDs' illumination and digitalized the signals, and a controller module that not only controlled the other modules but also ensured data storage, power management, and connectivity of the system. The system took advantage of the optical band selection that made it possible to develop an integrated system based on four discrete optical bands. The reflectance data collected in both lab and field environments revealed a variation of the optical signals along the ripening season, which was observed in the raw signal and also in PCA scores after analyzing the data through this multivariate technique. This variability was present in both red (cv. Touriga Nacional) and white (cv. Loureiro) grapes. We also identified some of the events that may affect optical monitoring in field conditions. Hence, this work focused on the design, characterization, and operation of the spectral sensing system, paving the ground for the autonomous monitoring of grape berry ripening.

Considering the interest in expanding the optical measurements herein described to other applications such as the monitoring of phenolic maturation parameters of grapes (e.g., anthocyanins) or the vine water status, additional customized versions of the proposed optical module are also under development. Monitoring the phenolic maturation parameters can be achieved through the interaction of chlorophyll fluorescence with the phenolic components of the grape's skin (Agati et al., 2005). Therefore, the implementation of fluorescence measurements in our current optical layout implies the use of optical filters to block the excitation light and assure that the emission signal of the chlorophyll (with typical emission bands around 690 and 740 nm) is the only source of photons that reaches the photodetector(s). In this regard, two recent reports from our project's team focused on different aspects of the monolithic integration of interference and absorption filters on thin-films amorphous silicon photodiodes for this particular application (Nikolaidou et al., 2022a; Nikolaidou et al., 2022b).

Regarding the monitoring of vine water status, it is based on the collection of reflectance signals from grapevine plant leaves. In contrast to the reflectance signals for grape ripening, measuring the reflectance of the leaf requires optical bands not only in the Vis/NIR but also in the IR range (Pampuri et al., 2021a). Hence, a version of the optical module that includes LEDs and photodetectors capable of operating at both Vis and IR spectral ranges was also prepared and it is currently under evaluation.

Future developments of the IoT spectral sensing system introduced here will include the development of prediction models for the quantitative analysis of the technology grape ripening parameters (Total Soluble Solids, pH, Total acidity) as well as the integration of the end-node in a WSN.

CRediT authorship contribution statement

Hugo M. Oliveira: Conceptualization, Data curation, Analysis, Funding acquisition, Experiments/Investigation, Methodology, Project

administration, Supervision, Validation, Visualization, Writing – original draft, Writing – review & editing. **Alessio Tugnolo:** Conceptualization, Data curation, Investigation, Methodology, Software, Validation, Visualization, Writing – original draft, Writing – review & editing. **Natacha Fontes:** Conceptualization, Funding acquisition, Investigation, Resources, Validation, Writing – original draft, Writing – review & editing. **Carlos Marques:** Conceptualization, Software, Validation, Writing – original draft, Writing – review & editing. **Álvaro Geraldes:** Conceptualization, Software, Validation, Writing – original draft, Writing – review & editing. **Sophie Jenne:** Investigation, Methodology, Validation, Visualization, Writing – review & editing. **Hans Zappe:** Funding acquisition, Supervision, Writing – review & editing. **António Graça:** Resources, Writing – review & editing. **Valentina Giovenzana:** Investigation, Methodology, Writing – review & editing. **Roberto Beghi:** Investigation, Methodology, Writing – review & editing. **Riccardo Guidetti:** Funding acquisition, Supervision, Writing – review & editing. **João Piteira:** Conceptualization, Funding acquisition, Investigation, Methodology, Project administration, Software, Supervision, Validation, Writing – original draft, Writing – review & editing. **Paulo Freitas:** Conceptualization, Funding acquisition, Project administration, Supervision, Validation, Writing – review & editing.

Declaration of competing interest

The authors declare the following financial interests/personal relationships which may be considered as potential competing interests: Joao Piteira has patent #WO2018172114 issued to International Iberian Nanotechnology Laboratory. Paulo Freitas has patent #WO2018172114 issued to International Iberian Nanotechnology Laboratory.

Data availability

Data will be made available on request.

Acknowledgements

The authors acknowledge the i-Grape project that has received funding from the European Union's Horizon 2020 Research and Innovation program under Grant Agreement number 825521. The authors also thank Sandra Maya and Patrícia Barroso for the illustrations.

Appendix A. Supplementary data

Supplementary data to this article can be found online at https://doi.org/10.1016/j.compag.2023.108599.

References

Agati, G., Pinelli, P., Cortes Ebner, S., Romani, A., Cartelat, A., Cerovic, Z.G., 2005. Nondestructive evaluation of anthocyanins in olive (Olea europaea) fruits by in situ chlorophyll fluorescence spectroscopy. J. Agric. Food. Chem. 53, 1354–1363. https://doi.org/10.1021/jf048381d.

Agati, G., Meyer, S., Matteini, P., Cerovic, Z.G., 2007. Assessment of Anthocyanins in Grape (Vitis vinifera L.) Berries Using a Noninvasive Chlorophyll Fluorescence Method. J. Agric. Food. Chem. 55, 1053–1061. https://doi.org/10.1021/jf062956k.

Agati, G., Traversi, M.L., Cerovic, Z.G., 2008. Chlorophyll Fluorescence Imaging for the Noninvasive Assessment of Anthocyanins in Whole Grape (Vitis vinifera L.) Bunches. Photochem. Photobiol. 84, 1431–1434. https://doi.org/10.1111/j.1751-1097.2008.00424.x.

Agati, G., D'Onofrio, C., Ducci, E., Cuzzola, A., Remorini, D., Tuccio, L., Lazzini, F., Mattii, G., 2013. Potential of a Multiparametric Optical Sensor for Determining in Situ the Maturity Components of Red and White Vitis vinifera Wine Grapes. J. Agric. Food. Chem. 61, 12211–12218. https://doi.org/10.1021/jf405099n.

dos Santos Costa, D., Oliveros Mesa, N.F., Santos Freire, M., Pereira Ramos, R., Teruel Mederos, B.J., 2019. Development of predictive models for quality and maturation stage attributes of wine grapes using vis-nir reflectance spectroscopy. Postharvest Biol. Technol. 150, 166–178. https://doi.org/10.1016/j.postharvbio.2018.12.010.

Ercoli, L., Mariotti, M., Masoni, A., Massantini, F., 1993. Relationship between nitrogen and chlorophyll content and spectral properties in maize leaves. Eur. J. Agron. 2, 113–117. https://doi.org/10.1016/S1161-0301(14)80141-X.

Fernández-Novales, J., Barrio, I., Diago, M.P., 2021. Non-Invasive Monitoring of Berry Ripening Using On-the-Go Hyperspectral Imaging in the Vineyard. Agronomy 11. https://doi.org/10.3390/agronomy11122534.

Ferrara, G., Marcotuli, V., Didonna, A., Stellacci, A.M., Palasciano, M., Mazzeo, A., 2022. Ripeness Prediction in Table Grape Cultivars by Using a Portable NIR Device. Horticulturae 8, 613.

Ferro, M.V., Catania, P., 2023. Technologies and Innovative Methods for Precision Viticulture: A Comprehensive Review. Horticulturae 9, 399.

Francisco, G.-S., Luis, G.-S., Juan, J.-M.-N., Raquel, M.-D., Manuel, N., 2017. Using Near-Infrared Spectroscopy in Agricultural Systems. In: Konstantinos, G.K., Jan, S. (Eds.), Developments in near-Infrared Spectroscopy. IntechOpen, Rijeka, Ch. 5.

Freitas, P., Piteira, J., 2018. A monitoring device, a system and a method for monitoring a status of fruits, In: WO2018172114.

Garcia-Hernandez, C., Medina-Plaza, C., Garcia-Cabezon, C., Blanco, Y., Fernandez-Escudero, J.A., Barajas-Tola, E., Rodriguez-Perez, M.A., Martin-Pedrosa, F., Rodriguez-Mendez, M.L., 2018. Monitoring the Phenolic Ripening of Red Grapes Using a Multisensor System Based on Metal-Oxide Nanoparticles. Front. Chem. 6, 131. https://doi.org/10.3389/fchem.2018.00131.

Giovenzana, V., Beghi, R., Malegori, C., Civelli, R., Guidetti, R., 2014. Wavelength Selection with a View to a Simplified Handheld Optical System to Estimate Grape Ripeness. Am. J. Enol. Vitic. 65, 117. https://doi.org/10.5344/ajev.2013.13024.

Giovenzana, V., Civelli, R., Beghi, R., Oberti, R., Guidetti, R., 2015. Testing of a simplified LED based vis/NIR system for rapid ripeness evaluation of white grape (Vitis vinifera L.) for Franciacorta wine. Talanta 144, 584–591. https://doi.org/10.1016/j.talanta.2015.06.055.

Gomes, V., Rendall, R., Reis, M.S., Mendes-Ferreira, A., Melo-Pinto, P., 2021. Determination of Sugar, pH, and Anthocyanin Contents in Port Wine Grape Berries through Hyperspectral Imaging: An Extensive Comparison of Linear and Non-Linear Predictive Methods. Appl. Sci. 11 https://doi.org/10.3390/app112110319.

González-Caballero, V., Sánchez, M.-T., Fernández-Novales, J., López, M.-I., Pérez-Marín, D., 2012. On-Vine Monitoring of Grape Ripening Using Near-Infrared Spectroscopy. Food Anal. Meth. 5, 1377–1385. https://doi.org/10.1007/s12161-012-9389-3.

Jenne, S., Zappe, H., 2023. Simulation of light interaction with seedless grapes. J. Sci. Food Agric. 103, 57–63. https://doi.org/10.1002/jsfa.12111.

Meyers, J.M., Dokoozlian, N., Ryan, C., Bioni, C., Vanden Heuvel, J.E., 2020. A New. Satellite NDVI-Based Sampling Protocol for Grape Maturation Monitoring, Remote Sens. https://doi.org/10.3390/rs12071159.

Navarro, E., Costa, N., Pereira, A., 2020. A Systematic Review of IoT Solutions for Smart Farming. Sensors 20, 4231.

Nikolaidou, K., Condelipes, P.G.M., Caneira, C.R.F., Krack, M., Fontes, P.M., Oliveira, H. M., Kovačič, M., Krč, J., Topič, M., Cardoso, S., Freitas, P.P., Chu, V., Conde, J.P., 2022a. Monolithically integrated optical interference and absorption filters on thin film amorphous silicon photosensors for biological detection. Sensors and Actuators b: Chemical 356, 131330. https://doi.org/10.1016/j.snb.2021.131330.

Nikolaidou, K., Oliveira, H.M., Cardoso, S., Freitas, P.P., Chu, V., Conde, J.P., 2022b. Monolithic Integration of Multi-Spectral Optical Interference Filter Array on Thin Film Amorphous Silicon Photodiodes. IEEE Sens. J. 22, 5636–5643. https://doi.org/10.1109/JSEN.2022.3150228.

OIV, 2022. Compendium of International Methods of Wine and Must Analysis, Paris.

Pampuri, A., Tugnolo, A., Bianchi, D., Giovenzana, V., Beghi, R., Fontes, N., Oliveira, H. M., Casson, A., Brancadoro, L., Guidetti, R., 2021a. Optical specifications for a proximal sensing approach to monitor the vine water status in a distributed and autonomous fashion. Biosystems Engineering 212, 388–398. https://doi.org/10.1016/j.biosystemseng.2021.11.007.

Pampuri, A., Tugnolo, A., Giovenzana, V., Casson, A., Guidetti, R., Beghi, R., 2021b. Design of cost-effective LED based prototypes for the evaluation of grape (Vitis vinifera L.) ripeness. Comput. Electron. Agric. 189, 106381 https://doi.org/10.1016/j.compag.2021.106381.

Pampuri, A., Tugnolo, A., Giovenzana, V., Casson, A., Pozzoli, C., Brancadoro, L., Guidetti, R., Beghi, R., 2022. Application of a Cost-Effective Visible/Near Infrared Optical Prototype for the Measurement of Qualitative Parameters of Chardonnay Grapes. Appl. Sci. 12, 4853. https://doi.org/10.3390/app12104853.

Pérez-Expósito, J.P., Fernández-Caramés, T.M., Fraga-Lamas, P., Castedo, L., 2017. VineSens: An Eco-Smart Decision-Support Viticulture System. Sensors (basel) 17. https://doi.org/10.3390/s17030465.

Ribera-Fonseca, A., Noferini, M., Jorquera-Fontena, E., Rombolà, A.D., 2016. Assessment of technological maturity parameters and anthocyanins in berries of cv. Sangiovese (Vitis vinifera L.) by a portable vis/NIR device. Sci. Hortic. 209, 229–235. https://doi.org/10.1016/j.scienta.2016.06.004.

Río Segade, S., Giacosa, S., Gerbi, V., Rolle, L., 2019. Chapter 1 - Grape Maturity and Selection: Automatic Grape Selection. In: Morata, A. (Ed.), Red Wine Technology. Academic Press, pp. 1–16.

Rocchi, L., Rustioni, L., Failla, O., 2016. Chlorophyll and carotenoid quantifications in white grape (Vitis vinifera L.) skins by reflectance spectroscopy. Vitis 55, 11–16. https://doi.org/10.5073/vitis.2016.55.11-16.

Savi, S., Poni, S., Moncalvo, A., Frioni, T., Rodschinka, I., Arata, L., Gatti, M., 2019. Destructive and optical non-destructive grape ripening assessment: Agronomic comparison and cost-benefit analysis. PLoS One 14, e0216421.

Song, D., Gao, D., Sun, H., Qiao, L., Zhao, R., Tang, W., Li, M., 2021. Chlorophyll content estimation based on cascade spectral optimizations of interval and wavelength characteristics. Comput. Electron. Agric. 189, 106413 https://doi.org/10.1016/j.compag.2021.106413.

Spachos, P., 2020. Towards a Low-Cost Precision Viticulture System Using Internet of Things Devices. IoT 1, 5–20.

Tardaguila, J., Stoll, M., Gutiérrez, S., Proffitt, T., Diago, M.P., 2021. Smart applications and digital technologies in viticulture: A review. Smart Agric. Technol. 1, 100005 https://doi.org/10.1016/j.atech.2021.100005.

Tugnolo, A., Giovenzana, V., Malegori, C., Oliveri, P., Casson, A., Curatitoli, M., Guidetti, R., Beghi, R., 2021. A reliable tool based on near-infrared spectroscopy for the monitoring of moisture content in roasted and ground coffee: A comparative study with thermogravimetric analysis. Food Control 130, 108312. https://doi.org/10.1016/j.foodcont.2021.108312.

Vrochidou, E., Bazinas, C., Manios, M., Papakostas, G.A., Pachidis, T.P., Kaburlasos, V.G., 2021. Machine Vision for Ripeness Estimation in Viticulture Automation. Horticulturae 7, 282. https://doi.org/10.3390/horticulturae7090282.

Weiss, M., Jacob, F., Duveiller, G., 2020. Remote sensing for agricultural applications: A meta-review. Remote Sens. Environ. 236, 111402 https://doi.org/10.1016/j.rse.2019.111402.

Wold, S., Sjöström, M., Eriksson, L., 2001. PLS-regression: a basic tool of chemometrics. Chemometrics Intell. Lab. Syst. 58, 109–130. https://doi.org/10.1016/S0169-7439(01)00155-1.

Xu, J., Gu, B., Tian, G., 2022. Review of agricultural IoT technology. Artificial Intelligence in Agriculture 6, 10–22. https://doi.org/10.1016/j.aiia.2022.01.001.

Zhang, X., Yang, J., Lin, T., Ying, Y., 2021. Food and agro-product quality evaluation based on spectroscopy and deep learning: A review. Trends Food Sci. Technol. 112, 431–441. https://doi.org/10.1016/j.tifs.2021.04.008.